J Geophys (1983) 53:155–162

Journal of Geophysics

Observation of Gravity Changes During the Passage of Cold Fronts

T. Müller[1] and W. Zürn[2]

Geophysical Institute, University of Karlsruhe, Hertzstr. 16, D-7500 Karlsruhe, Federal Republic of Germany

Abstract. Clear observations of small but abrupt changes in gravity during the passage of cold fronts are reported. Instrumental effects can be ruled out by special experiments. Simple models for the atmosphere show that the direction and the order of magnitude of the observed effects can be explained by changes in gravitational attraction of the sensor mass by the atmosphere or by downward acceleration of the ground due to the increasing air pressure. This is additional evidence for the high importance of meteorological causes for long-period seismic noise.

Key words. Gravity changes - Cold front - Seismic noise

Introduction

Meteorological phenomena are well known to be a major source of noise in measurements of ground motion. Research in earth tides has identified several physical mechanisms by which meteorological variables cause signals on gravity-, tilt- and strainmeter records (e.g. Slichter et al., 1979; Warburton and Goodkind, 1977; Große-Brauckmann, 1979; Herbst, 1976; Zschau, 1979; Agnew, 1979). Seismologists have also studied noise from meteorological sources and have concluded that these dominate at periods longer than about 40 s (e.g. Sorrells, 1971; Sorrells et al., 1971; Ziolkowski, 1973). Kisslinger (1960) studied seismograms showing effects associated with the passage of tornadoes.

This paper presents further evidence for the importance of meteorological noise in seismic records especially in the free mode band. Simple models of cold fronts help to understand the measured effects.

Observations

The LaCoste-Romberg Earth-Tide gravimeter ET 19 at Schiltach Observatory ($\varphi = 48° 20' N$, $\lambda = 8° 19' E$; Mälzer, 1976) is equipped with electrostatic feedback and is very similar to the IDA instruments (Agnew et al., 1976). Its output is bandpass filtered for the recording of seismic mantle waves and free modes of the Earth. The frequency response of this system is identical to the UCLA ultralong-period seismometer described by Nakanishi et al. (1976). The cutoff periods (−3 dB) are 120 and 7,200 s, respectively, for this channel and its response to a step in gravity (vertical acceleration) is shown in Fig. 1. The output signal is recorded digitally as well as on a monitor chart recorder with a speed of 2 or 3 cm/h. Temperature, precipitation and the variations of local atmospheric pressures inside and outside the mine are recorded on analog charts at 3 cm/h. The interior of the mine is separated from the outside by an airlock (Heil, 1983).

With very few exceptions (instrumental gliches once or twice per year) transient disturbances on the filtered output of the gravimeter are clearly correlated with barometric pressure changes outside the mine. Sinusoidal barometric pressure waves produced sinusoidal oscillations of the gravity record provided the frequency was in the filter passband. Steplike changes in barometric pressure produced signals resembling closely the free

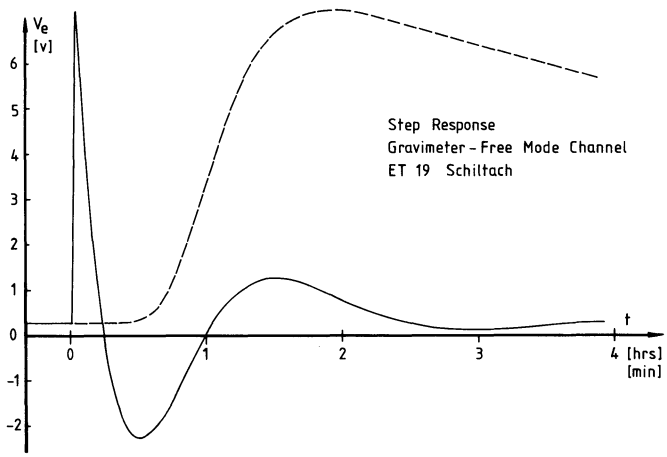

Fig. 1. Response of the free mode channel of LaCoste-Romberg tidal gravimeter ET 19 with electrostatic feedback. A sudden decrease in gravity of 10 μgal was simulated by instantaneously adding 110 mV to the feedback voltage. The step occurred at most one second after $t = 0$. Time scale in hours for solid line, in minutes for broken line

1 Present address: Prakla-Seismos, Postfach 510530, D-3000 Hannover 51, Federal Republic of Germany

2 Permanent address: Schiltach Observatory, Heubach 206, D-7620 Wolfach, Federal Republic of Germany

Offprint requests to: W. Zürn

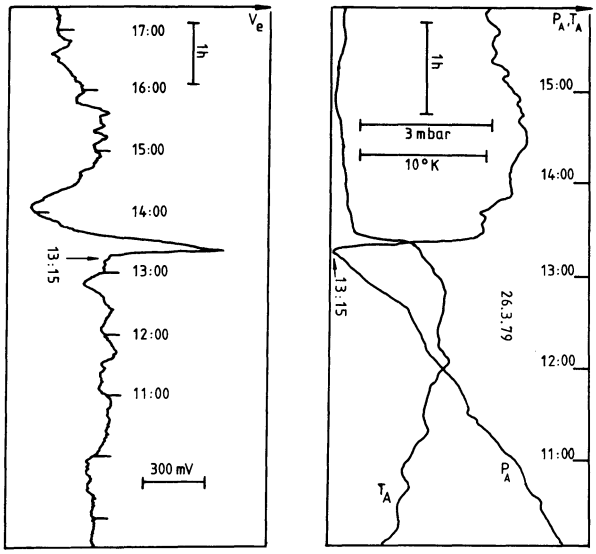

Fig. 2. Cold front passage on 26 March 1979. Simultaneous analog records of external pressure p_A, temperature T_A (*right*) and gravimeter output voltage V_e (*left*). In the center of the passband the sensitivity is 805 mV/μgal. Different time scales were used and time is increasing from bottom to top

mode channel's step response. Figures 2 to 5 and 11 show examples. The more the pressure change resembles a step, the closer the gravimeter output looks like the response to a step in gravity (Fig. 1). Figures 2, 3 and 4 show selected signals associated with the passage of cold fronts. The weather maps for times bracketting our signals confirm, that in each case a cold front was indeed moving through SW-Germany.

The polarity of the pulses always corresponded to a decrease in gravity when outside pressure increased. In Fig. 3 the detrimental effect of such a cold front pulse on the recording of free oscillations of the earth excited by an earthquake about 14 h earlier is demonstrated.

Figures 4 and 5 show more complicated behaviour of atmospheric pressure associated with thunderstorm activity. Every large disturbance has its clear counterpart in the gravity record. Figure 6 shows, for comparison, the signals in three components from the very-long period channels of Wielandt-Streckeisen seismometers (Wielandt and Streckeisen, 1982). The signals on the horizontal components are about ten times larger than on the vertical components. Figure 11 shows a fine example of quasiperiodic pressure variations and their effect on gravity due to the pressure wave from the

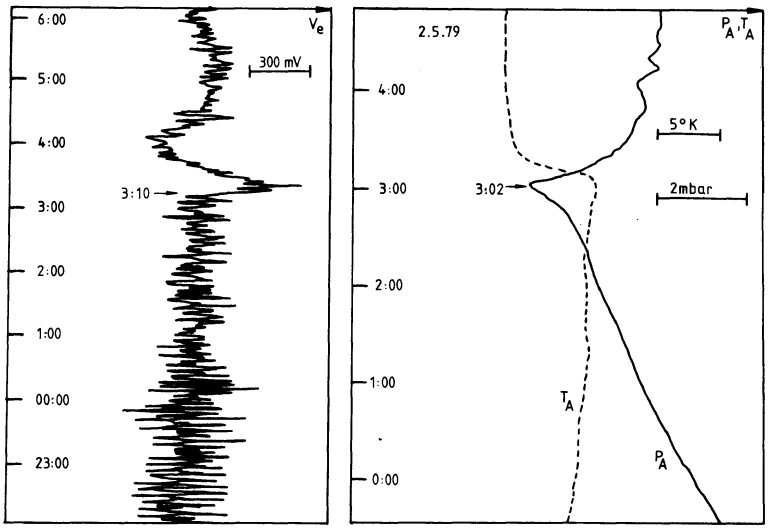

Fig. 3. Cold front passage on 2 May 1979. Simultaneous analog records of external and internal pressures p_A, p_i and temperature T_A (*right*) and gravimeter output voltage V_e (*left*). Different time scales were used and time increases from bottom to top. The cold front effect is superimposed on decaying free oscillations of the Earth excited by an earthquake in the Loyalty Islands region ($m_b = 7.2$; Origin time 13:03:37.1, 1 May)

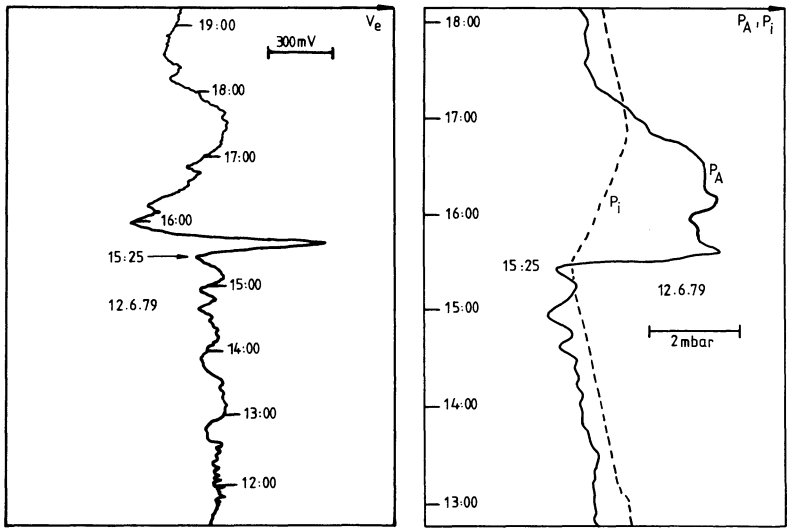

Fig. 4. Same as Fig. 2 and 3 for cold front passage on 12 June 1979. Note the difference in gravimeter response to the rise and fall-off of pressure. The reaction to the rise is a step-response, while the reaction to the fall-off is very smooth. The time scale of the fall-off is a factor of five larger than for the rise and most of its energy lies outside the passband of this channel

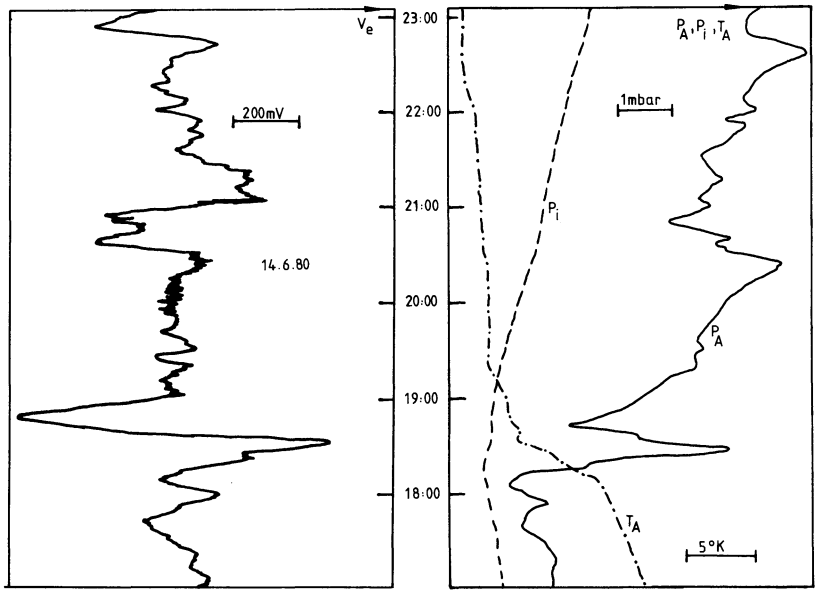

Fig. 5. Same as Figs. 2, 3 and 4 for cold front passage on 14 June 1980 associated with thunderstorms. Correlation between p_A and V_e is quite clear. The records of p_i and p_A demonstrate the lowpass properties of the air-lock

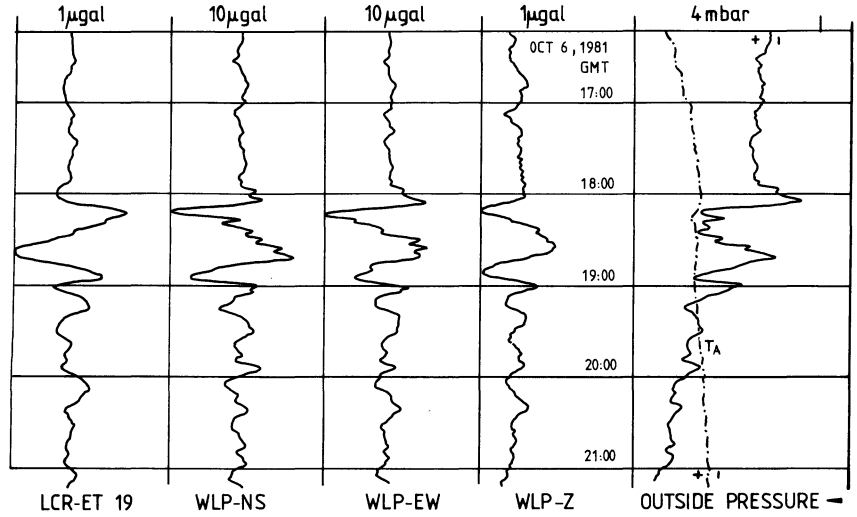

Fig. 6. Simultaneous records of outside pressure p_A and temperature T_A (analog, *right*) and bandpassed vertical and horizontal accelerations (reproduced from digital tape). The traces denoted WLP are from three Wielandt-Streckeisen seismometers (very long period channels). Scales are only valid for center of passbands, different scales for vertical and horizontal components are used. Polarity is reversed between WLP-Z and LCR-ET 19 and small differences in the response of these two vertical components are due to differences in the transfer functions of these instruments

Mount St. Helens eruption of May 1980 (see also Ritsema, 1980; Bolt and Tanimoto, 1981; Bath, 1982).
On Figs. 4 and 5 the temporal variation of inside pressure p_i can also be seen. There are at most minute changes of pressure near the instruments and we demonstrate in the next section that these cannot cause the observed effect.

The direct output of the gravimeter (tidal channel) has 70 times less amplification (at much larger bandwidth), therefore we could not detect the pressure induced transients on the tide records. Also we could never detect pulses during the passage of warm fronts, in this case pressure changes very smoothly.

Gravimeter Sensitivity to Ambient Air Pressure Changes

A variety of physical mechanisms could allow variations in ambient air pressure to produce apparent gravity variations at the output of the instrument: deformation of the instrument case, thermal deformations caused by pressure-induced temperature variations, imperfect sealing and buoyancy compensation etc. Two types of experiments were performed to detect such a sensitivity to ambient air pressure.
An air-lock with a time constant of about 4 h (Heil, 1983) separates the interior of the mine from the outside. Fast pressure variations are reduced appreciably in the interior (see Figs 3, 4 and 6), while slow pressure variations are only slightly attenuated and delayed in phase.
When outside pressure (p_A) changes steadily for some time this phase lag leads to small, time-dependent pressure differences across the air-lock. If, in this situation, both doors of the lock are opened, inside pressure p_i changes to outside pressure immediately. In this way steps Δp_i of a few mbars can be produced at constant p_A. Such tests were carried out several times with steps of $\Delta p_i \sim 2$–7 mbars without any indication of a response of the instrument, one example is shown in Fig. 7.

Another test was performed by opening the valves of two large cylinders of compressed air in the interior

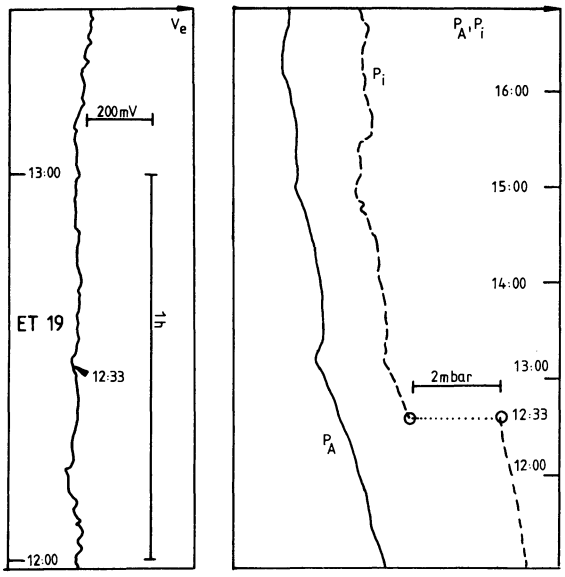

Fig. 7. Same as Fig. 2, 3, 4 and 5 for air-lock test at 12:33 GMT. There is no reaction in the gravity record for this step in p_i of about 2 mbar

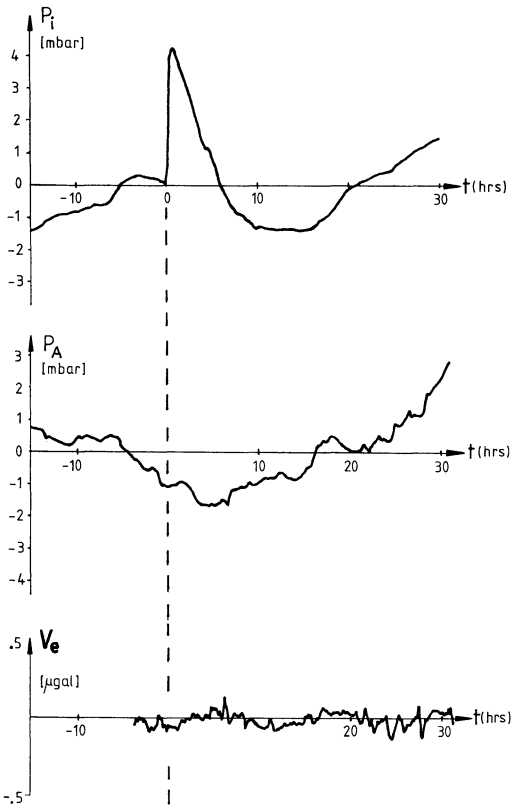

Fig. 8. Release of compressed air in the interior of the mine. Simultaneous records of inside and outside pressure, p_i and p_A and gravimeter output converted to μgal. Gravimeter does not react visibly, although the rise time of the transient in p_i is 30 min, in the passband of the free mode filter

with the air-lock closed. This caused a quick rise in inside pressure and a slow drop because of the long time-constant of the air-lock (for more details see Heil, 1983). As is seen in Fig. 8 the gravimeter did not respond to this pulse in Δp_i either.

For changes of outside pressure of the same order of magnitude there clear signals. Therefore instrumental sensivity to ambient air pressure can be ruled out as an explanation of the observations. These must be due to Newtonian attraction and/or crustal deformation by the changing atmosphere.

Models of Cold Fronts

Contributions to gravity from Newtonian attraction and crustal deformation by air masses were evaluated for the temporal change of density in an otherwise constant layer of air by Slichter et al. (1979), for moving vertical circular cylinders of air (pressure cells) by Warburton and Goodkind (1977), Block and Moore (1966) and Müller (1981) and for spherical harmonic distribution of air pressure by Spratt (1982). In all cases it turned out that for a gravimeter the effect of Newtonian attraction is 5 to 10 times larger than the effect of crustal deformation. However, all these models appear inadequate to describe the transient effects of moving fronts.

Our models consist of two isothermal air masses above ($z>0$) a rigid Earth separated by either a sharp vertical plane or a sharp hyperbolic surface. The gravimeter rests at $x=x_A$, $y=z=0$. The density of each air mass is assumed to vary with height z according to:

$$\rho(z)=\rho_0 \exp(-z/H) \tag{1}$$

where $H=7.99\cdot 10^3$ m is the scale height used. The models are depicted in Fig. 12.

The two air masses differ only by their densities ρ_0 at ground level (ρ_+-cold air, ρ_--warm air). The intersection of the front with the surface is x_F with cold air at $x\leqq x_F$. The models are two-dimensional, no model property depends on y; the front later moves in the positive x-direction with speed v_F. The gravitational attraction of this atmosphere at the site of the gravimeter (gravity positive downward):

$$g(x_A) = -G\int_{z=0}^{\infty}\int_{x=-\infty}^{\infty}\int_{y=-\infty}^{\infty}\frac{\rho_0(x)\exp(-z/H)\,z\,dx\,dy\,dz}{([x-x_A]^2+y^2+z^2)^{3/2}} \tag{2}$$

where G is the gravitational constant.

In our first model the front is a vertical plane ($x=x_F$). In this case the integral Eq. (2) can be evaluated analytically. The result is (see Appendix):

For $x_F-x_A=a\geqq 0$

$$g(x_A)=-2GH\rho_+ \cdot\left\{\pi+\left(1-\frac{\rho_-}{\rho_+}\right)\left\{\mathrm{ci}\left(\frac{a}{H}\right)\sin\left(\frac{a}{H}\right) +\mathrm{si}\left(\frac{a}{H}\right)\cdot\cos\left(\frac{a}{H}\right)\right\}\right\}, \tag{3a}$$

and for $x_F-x_A=a\leqq 0$

$$g(x_A) = -2GH\rho_+ \cdot \left\{\pi\frac{\rho_-}{\rho_+} - \left(1-\frac{\rho_-}{\rho_+}\right)\left\{\mathrm{ci}\left(\frac{|a|}{H}\right)\sin\left(\frac{|a|}{H}\right) + \mathrm{si}\left(\frac{|a|}{H}\right)\cos\left(\frac{|a|}{H}\right)\right\}\right\}, \quad (3b)$$

where

$$\mathrm{ci}(x) = \int_x^\infty \frac{\cos u}{u}\,du,$$
$$\mathrm{si}(x) = -\int_x^\infty \frac{\sin u}{u}\,du \quad (4)$$

are modified cosine and sine integrals. The functions $g(x_A)$ is symmetrical about the point $x_A = x_F$, $g(x_F) = -GH\pi(\rho_+ + \rho_-)$ and has the asymptotic values $-2GH\pi\rho_-$ for $x_A \gg x_F (a \ll 0)$ and $-2\mathrm{GH}\pi\rho_+$ for $x_A \ll x_F (a \gg 0)$. The latter expressions correspond to the gravitational attraction at the bottom of either an isothermal atmosphere (Eq. (1)) with infinite extent or a homogeneous atmosphere ($\rho = \mathrm{const} = \rho_0$) with finite vertical extent H.

The second model uses a more realistic shape of the front, which is now a branch of a hyperbola given by:

$$x_F(z) = -a_1[(1 + z^2/a_2^2)^{1/2} - 1] + x_F(0) \quad (5)$$

where a_1, a_2 are parameters of the hyperbola describing the slope $s = a_1/a_2$ for large z and the distance a_1 between the intersections with the ground level of the hyperbola and its asymptote ($2a_1$: transverse axis, $2a_2$: conjugate axis of hyperbola). This simulates how the cold air near the front is underlying the less dense warm air. A typical slope is $s = 100$ (Liljequist and Cehak, 1979). For this model the final integration over z (Eq. (A4)) has to be done numerically, because $x_F = x_F(z)$. The step size used was $\Delta z = 25$ m and the integration was truncated at an altitude of 30 km. This truncation leads to an error of about 10% in the total signal for an infinite isothermal atmosphere, our model is physically doubtful at this level anyway. The curvature of the front near ground level, defined by a_1 and a_2 has a strong influence on the gravity signal, because it modifies the abruptness with which cold air replaces warm air directly above the gravimeter. We chose $a_1 = 300$ km by comparison with meteorological literature (Liljequist and Cehak, 1979).

Both models result in a function which depends on the relative positions of the front and the gravimeter $x_F(0) - x_A$. If the front moves with velocity v_F along the x-direction, the gravimeter senses a gravity variation with time $\Delta g(x_A, t)$ in Fig. 9 and 10. These time functions were convolved with the step response of the instrument (Fig. 1) to yield its output signal $V_e(t)$. Figure 9 and 10 show results for the vertical and hyperbolic front models, respectively. Typical front velocities are of the order of 10 to 20 ms^{-1} (Müller, 1981). As Fig. 9 shows the speed of the front is an important factor for the amplitude of the transient because of the limited bandwidth of the instrument.

The amplitude of the pulse for a given model depends linearly on the density difference at ground level $\Delta\rho = \rho_+ - \rho_-$. For the observed transients the observed

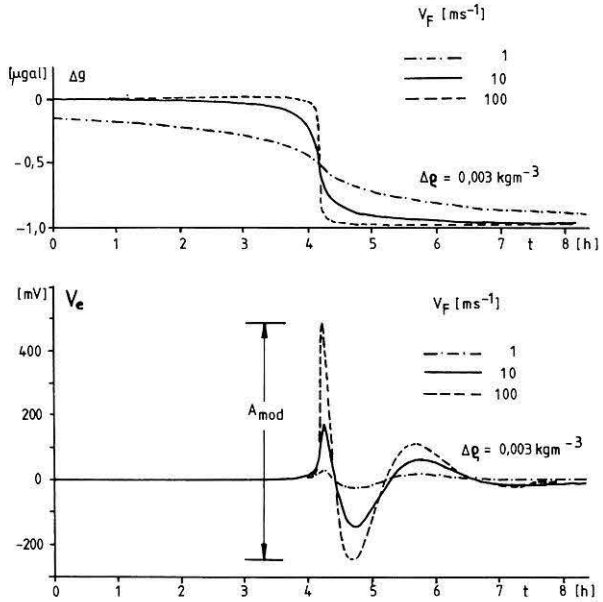

Fig. 9. Cold front model with vertical plane boundary. Top: change of gravity as sensed by the gravimeter mass as a function of time computed for $\Delta\rho = 0.003$ kg m^{-3} and three different front speeds. Corresponding signals at the bottom (805 mV/μgal). Amplitudes A_{mod} are used in Table 1

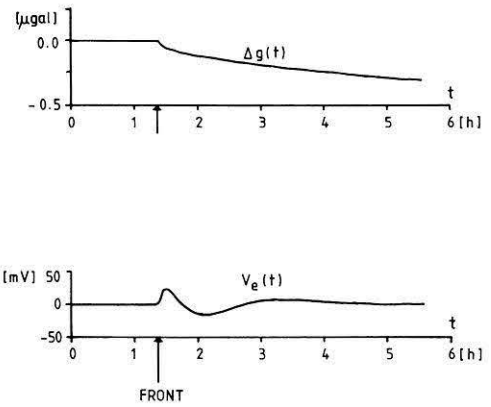

Fig. 10. Cold front model with hyperbolic front using $\Delta\rho = 0.003$ kg m^{-3}, $v_F = 10$ ms^{-1}, $s = 100$ and $a_1 = 3 \cdot 10^5$ m. Otherwise same as Fig. 10. The amplitude of the signal in this case is much lower than for the model in Fig. 9

pressure increase and temperature drop at the passage of the front were used to compute $\Delta\rho$ from the ideal gas law:

$$P_A/\rho_0 = R \cdot T_A. \quad (7)$$

In Table 1 we compare measured peak-to-peak amplitudes A_{obs} for clear cold front passages (like in Fig. 2 and 3) with amplitudes computed as described above for the hyperbolic model using $v_F = 10$ ms^{-1}, $a_1 = 300$ km and $s = 100$ and $\Delta\rho$ computed by Eq. (7). The ratio of observed to computed amplitudes is close to one in all cases. Of course, this agreement must be considered to be somewhat fortuitous because of the assumptions and simplifications implied in the model. But this clearly shows that Newtonian attraction alone

Table 1. Comparison of observed and computed peak-to-peak amplitudes of gravimeter response to cold front passages with simple temporal pressure changes. Δp, ΔT and A_{OBS} are observed data; Δp is computed using the ideal gas law Eq. (7) and A_{MOD} is computed as described in the text for the hyperbolic front model ($\Delta\rho$, $s=100$, $a_1=3\cdot10^5$ m, $v_F=10\,\mathrm{ms}^{-1}$)

Date	Δp_A [mbar]	$-\Delta T_A$ [°K]	$\Delta\rho$ [kg·m^{-3}]	A_{obs} [mV]	A_{mod} [mV]	A_{obs}/A_{mod}
16Mar 1978	2.1	5.7	0.030	525	630	0.83
26 Mar 1978	2.9	4.2	0.024	615	504	1.22
11 Sep 1978	2.7	5.0	0.028	645	588	1.10
9 Mar 1979	2.7	3.5	0.016	495	336	1.47
26 Mar 1979 (Fig. 2)	3.3	7.5	0.041	960	856	1.12
2 May 1979 (Fig. 3)	2.4	6.2	0.032	720	672	1.07
15 Dec 1979	1.7	3.2	0.018	500	378	1.32
2 Apr 1980	1.3	2.7	0.014	380	294	1.29

can account for shape, amplitude and polarity of the observations.

Other contributions to the gravity change sensed by the gravimeter are produced by downward displacement of the surface of the Earth by increasing air pressure:

a) downward motion of the gravimeter in the Earth's gravity field, $\Delta g=-\Delta z\cdot(\partial g/\partial z)_0$;

b) downward displacement of the equipotential surfaces of the Earth's gravity field due to the displaced masses;

c) the inertial effect on the gravimeter mass by the downward acceleration, $\Delta g=(d^2\Delta z/dt^2)$.

The first effect causes an increase, the last two a decrease in gravity. From the observations it is clear that either Newtonian attraction or effects *b* and *c* overwhelm effect *a*. At periods much less than one hour, effect *c* is larger than effect *a* for any displacement, given the gradient of gravity is not much larger than 300 μgal/m. For these reasons the inertial effect (*c*) only must be considered as an alternative explanation, at least for higher frequencies.

For the cold front passages it is impossible to estimate the peak downward acceleration of the ground from the local pressure record. However, an estimate for the quasi-sinusoidal pressure variations in Fig. 11 can be derived. Sorrels (1971, Eq. (24)) has calculated the vertical displacement at the surface of an isotropic, homogeneous elastic halfspace (Lamé parameters λ, μ) due to a pressure wave of amplitude P_0, frequency $\omega_0/2$ and speed C_0 propagating in *x*-direction under the assumption that $C_0 \ll v_s, v_p$ (elastic velocities of the halfspace)

$$W=\frac{C_0 P_0(\lambda+2\mu)}{2\mu(\lambda+\mu)}\frac{1}{|\omega_0|}\cdot\exp(i\omega_0(t-x/C_0)). \tag{8}$$

The peak acceleration is then:

$$|\Delta g_{\max}|=\left|\frac{d^2w}{dt^2}\right|_{\max}=C_0\omega_0 P_0\frac{\lambda+2\mu}{2\mu(\lambda+\mu)}. \tag{9}$$

From Fig. 11 we get for the largest signal with $\lambda=\mu$, $\mu=2.3\cdot10^{10}\,\mathrm{kg\,m^{-1}\,s^{-2}}$ (granite $V_p=5.2\cdot10^3\,\mathrm{ms}^{-1}$, $\rho=2.6\cdot10^3\,\mathrm{kgm}^{-3}$), $P_0=0.23\cdot$mbar, $C_0=308\,\mathrm{ms}^{-1}$,

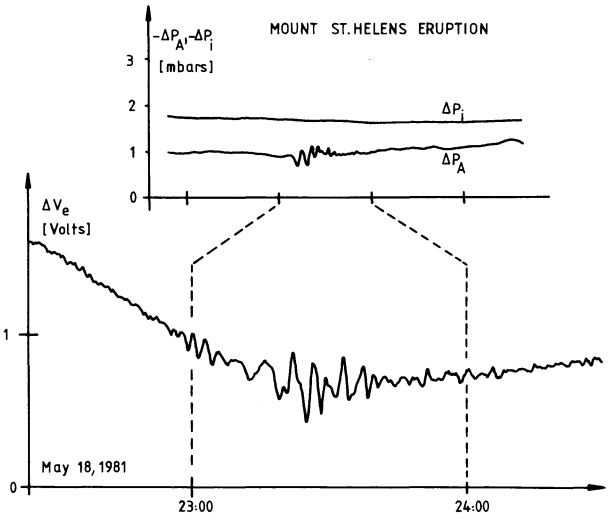

Fig. 11. Simultaneous records of p_A and V_e (805 mV/μgal) on 18 May 1980. The pressure wave from the eruption of Mount St. Helens can clearly be seen on the pressure and gravity records. The first arrival corresponds to a velocity of 308 m s^{-1} along the great circle. The wave train arriving shortly before 23:00 GMT is probably Rayleigh wave R_2 from an earthquake in Yugoslavia ($m_5=5.8$, *O.T.* 20:02:57.5); the long period trend is from nonlinear gravimeter response to R_1 of that quake

$2\pi/\omega_0=4.33$ min a peak-to-peak acceleration of 0.56 μgal. The observed amplitude is 426 mV$_{pp}$, corresponding to 0.53 μgal. Again this very good agreement is somewhat fortuitous because of simplifications. A more realistic crustal model would reduce the theoretical acceleration appreciably.

For warm fronts the pressure records never showed fast changes and neither were gravity signals observed. Although the same total pressure change might occur, it does so much more slowly and therefore the corresponding gravity signals do not come through the passband of the filter with measureable amplitude. This was confirmed by model calculations (Müller, 1981).

Figure 5 and 6 show very complicated frontal passages associated with thunderstorms. In those cases our models are much too simple. In this case additional effects may contribute to the gravity signal, which are

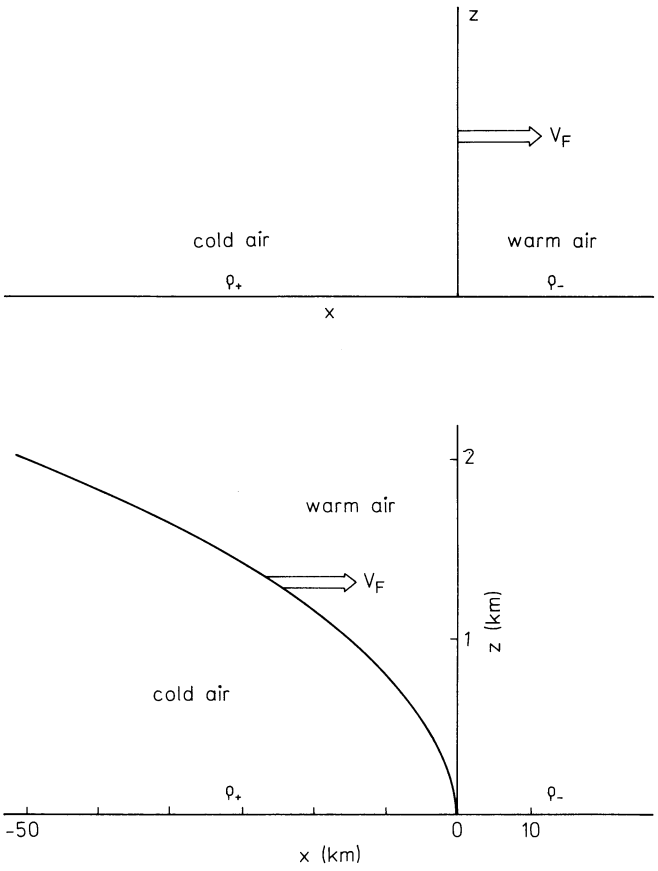

Fig. 12. Two cold front models used in calculations. Note difference in vertical and horizontal scale for hyperbolic front

very hard to estimate: such as vertical motion of air masses, turbulence and heavy rains.

Conclusions

The observed pressure-correlated gravity transients during the passage of cold fronts at the Schiltach underground observatory can be explained in shape, polarity and magnitude by the direct gravitational attraction of the sensor mass by air masses of different densities. The only competing mechanism at higher frequencies ($\gtrsim$4 mHz) is the inertial effect due to vertical acceleration of the ground by the pressure changes. Since our signals were clearly above the normal vertical seismic noise level in the free mode band, we conclude that this noise is caused by the same effects at more moderate amplitudes of pressure or density variations in the atmosphere. Therefore the quality of a record from such an instrument, for example from the IDA-network, depends on local weather. One cannot expect, on average, top-quality vertical seismic records at very long periods from stations where the weather is notoriously bad in terms of frequent large fluctuations in barometric pressure.

For horizontal seismic noise at these frequencies the situation is even worse. According to Große-Brauckmann (1979) the contribution to tilts of the deformation effect is dominant over the gravitational attraction. The latter is of the same order of magnitude for vertical and horizontal instruments, therefore long period horizontal seismic noise should be larger than vertical noise, when caused by the atmosphere. This is demonstrated in Fig. 6, where pressure-correlated signals are ten times larger for horizontal components.

Our simple models cannot be used to prove definitely that Newtonian attraction is the dominant mechanism for the cold front signals in gravity. But since we had to over-estimate the inertial effect to match the observed amplitude at rather high frequency and because this effect decreases linearly with decreasing frequency we feel that Newtonian attraction is highly likely to be dominant. The rise-times of the pressure signals in all cases were larger than the period for which the inertial effect became comparable. The relative importance of the mechanisms must be site-dependent due to the changing crustal structure and topography of the surface could have an influence also. Therefore it is not possible to draw conclusions of more general nature, but we have demonstrated that Newtonian attraction could explain the observed signals and that appreciable contributions must be expected from the inertial effect due to the deformation of the crust.

Appendix: Derivation of Eq. (3)

Equation (2) has to be solved in the case of the vertical front with

$$\rho_0(x)=\begin{cases}\rho_+ & x<x_F \text{ cold, denser air}\\ \rho_- & x_F<x \text{ warm air.}\end{cases} \tag{A 1}$$

The integration over coordinate y results in:

$$\int_{y=-\infty}^{+\infty}[(x-x_A)^2+y^2+z^2]^{-3/2}\,dy = 2[(x-x_A)^2+z^2]^{-1}. \tag{A 2}$$

Then the integral over x is:

$$\int_a^b[(x-x_A)^2+z^2]^{-1}\,dx=\frac{1}{z}\operatorname{atan}\left(\frac{x-x_A}{z}\right)\Big|_a^b. \tag{A 3}$$

The principal values have to be taken for the atan-function as $a\to-\infty$ and $b\to+\infty$.

$$\begin{aligned}g(x_A)&=-2G\int_{z=0}^{\infty}\exp\left(-\frac{z}{H}\right)\left[\rho_+\left(\operatorname{atan}\frac{x_F-x_A}{z}+\frac{\pi}{2}\right)\right.\\&\quad\left.+\rho_-\left(\frac{\pi}{2}-\operatorname{atan}\frac{x_F-x_A}{z}\right)\right]dz\\&=-2G\left\{\frac{\pi}{2}(\rho_++\rho_-)\int_{z=0}^{\infty}\exp\left(-\frac{z}{H}\right)dz\right.\\&\quad\left.+(\rho_+-\rho_-)\int_0^{\infty}\exp\left(-\frac{z}{H}\right)\operatorname{atan}\frac{x_F-x_A}{z}\,dz\right\}\end{aligned}$$

$$\begin{aligned}g(x_A)&=-2G\left\{\frac{\pi}{2}(\rho_++\rho_-)H\right.\\&\quad\left.+(\rho_+-\rho_-)\int_{z=0}^{\infty}\exp\left(-\frac{z}{H}\right)\operatorname{atan}\frac{x_F-x_A}{z}\,dz\right\}\end{aligned} \tag{A 4}$$

and by partial integration using the abbreviation $a = x_F - x_A$

$$g(x_A) = -2G\left\{\frac{\pi}{2} H(\rho_+ + \rho_-) - H(\rho_+ - \rho_-) e^{-z/H} \operatorname{atan} \frac{a}{z}\Big|_0^\infty - H(\rho_+ - \rho_-) a \int_0^\infty \frac{\exp(-z/H)\, dz}{z^2 + a^2}\right\}. \quad \text{(A5)}$$

At this point the cases $a > 0$ and $a < 0$ must be distinguished for two reasons. Firstly the second term is:

$$\lim_{z \to 0} \left(\operatorname{atan} \frac{a}{z}\right) = \begin{cases} \pi/2 & a > 0 \\ 0 & a = 0 \\ -\pi/2 & a < 0. \end{cases}$$

Secondly the third term can be interpreted as a Laplace Transform if $\mathrm{Re}(a) > 0$, $\mathrm{Re}(s) > 0$ (Erdélyi et al., 1954):

$$L\{(t^2 + a^2)^{-1}\} = -\frac{1}{a}\{\mathrm{ci}(as) \cdot \sin(as) + \mathrm{si}(as) \cdot \cos(as)\}$$

where $\mathrm{ci}(x)$, $\mathrm{si}(x)$ are defined in Eq. (4). Hence for $a > 0$ and $s = 1/H$, Eq. (3a) and for $a < 0$, Eq. (3b) result. For $a = 0$ $g(x_A) = -GH\pi(\rho_+ + \rho_-)$.

Acknowledgements. We would like to thank H. Otto and W. Großmann for maintenance of the instrumentation and the air-lock and for help with the active experiments. Drs. D. Emter, G. Müller, E. Wielandt and H. Wilhelm made many helpful comments on the manuscript. Discussions with Drs. H. Dieterich, Frankfurt and F. Fiedler, Karlsruhe helped us to understand meteorological phenomena a little better. E. Heil and E. Wielandt provided material for Fig. 6 and 8. P. Illich helped with the figures and H. Gadau typed the manuscript. The Deutsche Forschungsgemeinschaft supported this research under grants Zu 35/1-4 and B5-SFB 108. All this is gratefully acknowledged.

References

Agnew, D.C., Berger, J., Buland, R., Farrell, W., Gilbert, F.: IDA network for very long period seismology. EOS (Trans. Am. Geophys. Un.) **57**, 180–188, 1976

Agnew, D.C.: Strain tides at piñon Flat: analysis and interpretation. Ph. D. Thesis, University of California at San Diego, 1979

Bath, M.: Atmospheric waves from Mount St. Helens. EOS (Trans. Am. Geophys. Un.) **63**, 193, 1982

Block, B., Moore, R.D.: Measurements in the Earth mode frequency range by an electrostatic sensing and feedback gravimeter. J. Geophys. Res. **71**, 4361–4375, 1966

Bolt, B.A., Tanimoto, T.: Atmospheric oscillations after the May 18, 1980 eruption of Mount St. Helens. EOS (Trans. Am. Geophys. Un.) **62**, 529, 1981

Erdélyi, A., Magnus, W., Oberhettinger, F., Tricomi, F.G.: Tables of integral transforms, Vol. I. New York : McGraw-Hill, 1954

Große-Brauckmann, W.: Untersuchungen der Bodenunruhe im Periodenbereich von 2 min–1 h mit dem Askania Bohrlochneigungsmesser. Ph. D. Thesis, Clausthal Techn. University, 1979

Heil, E.: Erfahrungen mit einem Vertikalextensometer im Observ. Schiltach. Ph. D. Thesis, Karlsruhe University, 1983

Herbst, K.: Interpretation von Neigungsmessungen im Periodenbereich oberhalb der Gezeiten. Ph. D. Thesis, Clausthal Tech. University, 1976

Kisslinger, C.: Seismograms associated with the near passage of tornados. J. Geophys. Res. 65, 721–728, 1960

Liljequist, G.H., Cehak, K.: Allgemeine Meteorologie, 385 pp., Vieweg und Sohn, Braunschweig, 1979

Mälzer, H.: The Observatory. In: Proc. Seventh Int. Symposium Earth Tides (Ed. Szadeczky-Kardoss), 725–727, Schweizerbart'sche Verlagsbuchhandlung, Stuttgart, 1976

Müller, T.: Die Untersuchung von langperiodischen Schweresignalen beim Durchzug von Wetterfronten. Diploma Thesis, Karlsruhe University, 1981

Nakanishi, K.K., Knopoff, L., Slichter, L.B.: Observation of Rayleigh wave dispersion at very long periods. J. Geophys. Res. **81**, 4417–4421, 1976

Ritsema, A.R.: Observation of St. Helens eruption. EOS (Trans. Am. Geophys. Un.) **61**, 1201, 1980

Slichter, L.B., Zürn, W., Syrstad, E., Knopoff, L., Smythe, W.D., Uffelman, H.: Long period gravity tides at the South Pole. J. Geophys. Res. **74**, 6207–6212, 1979

Sorrells, G.G.: A preliminary investigation into a relationship between long-period seismic noise and local fluctuations in the atmospheric pressure field. Geophys. J.R. Astron. Soc. **26**, 71–82, 1971

Sorrels, G.G., McDonald, J.A., Der, Z.A., Herrin, E.: Earth motion caused by local atmospheric pressure changes. Geophys. J.R. Astron. Soc. **26**, 83–98, 1971

Spratt, R.S.: Modelling the effect of atmospheric pressure variations on gravity. Geophys. J.R. Astron. Soc. **71**, 173–186, 1982

Warburton, R.J., Goodkind, J.M.: The influence of barometric-pressure variations on gravity. Geophys. J.R. Astron. Soc. **48**, 281–292, 1977

Wielandt, E., Streckeisen, G.: The leaf-spring seismometer-design and performance. Bull. Seismol. Soc. Am. **72A**, 2349–2368, 1982

Ziolkowski, A.: Prediction and suppression of long-period non-propagating seismic noise. Bull. Seismol. Soc. Am. **63**, 937–958, 1973

Zschau, J.: Air pressure induced tilt in porous media. In: Proc. Eighth Int. Symp. Earth Tides Bonatz, Melchior, eds.: pp. 418–433, Bonn, 1979

Received April 27, 1983; Revised version June 20, 1983
Accepted June 20, 1983